Room-Temperature Chemical Synthesis of Silver Telluride Nanowires

A. K. Samal and T. Pradeep*

DST Unit on Nanoscience (DST UNS), Department of Chemistry and Sophisticated Analytical Instrument Facility, Indian Institute of Technology, Madras, Chennai 600 036 India

Received: March 03, 2009; Revised Manuscript Received: May 21, 2009

We have developed a room-temperature solution-phase route for the preparation of one-dimensional silver telluride nanowires (Ag_2Te NWs). The Ag_2Te NWs of 600 nm length and 20 nm diameter were synthesized by the reaction of tellurium nanowires (Te NWs) with silver nitrate ($AgNO_3$) in water. We propose that Te NWs act as the template and the reducing agent simultaneously, enabling the formation of polycrystalline Ag_2Te NWs. Various microscopic and spectroscopic tools, such as HRTEM, SEM, EDAX, XRD, DSC, XPS, and Raman, were used for the characterization of Ag_2Te NWs. The phase transition corresponding to the structural transition from the low-temperature monoclinic phase to the high-temperature face-centered cubic phase occurs at 417.7 K. We studied the electrical resistance and investigated the influence of temperature on the thermal emf. The Seebeck coefficient showed a maximum of $\sim$142 μV K^{-1}, a value much higher than that of the bulk material and thin films (65−130 μV K^{-1}). A surface-enhanced Raman scattering investigation of dispersed Ag_2Te NWs showed them to be sensitive up to 10^{-7} M crystal violet. The monodispersity and the homogeneity of the NWs through a simple solution-phase protocol would pave the way for further studies and applications.

Downloaded by INDIAN INST OF TECH MADRAS on July 31, 2009
Published on July 8, 2009 on http://pubs.acs.org | doi: 10.1021/jp901953f

Introduction

Recently, considerable attention has been paid to the synthesis of semiconducting one-dimensional (1D) nanowires (NWs) due to their potential applications in electronics and optoelectronics.[1,2] The development of proper synthetic procedures can enhance the optical, electronic, magnetic, and thermal properties of such NWs. Such materials can be used for the development of nanodevices, sensors, and magnetic memories.[3] Silver chalcogenides, particularly Ag_2Te, have been receiving tremendous attention due to their interesting semiconducting properties.[4−7] In addition, Ag_2Te is known to show a phase transition from the low-temperature monoclinic phase (β-Ag_2Te) to the high-temperature face-centered cubic phase (α-Ag_2Te) at $\sim$423 K.[8−10] Low-temperature β-Ag_2Te is a narrow band gap semiconductor with high electron mobility and low lattice thermal conductivity.[11] In the α-Ag_2Te phase, silver cations can move freely, which enhances the conductivity, leading to superionic conductivity.[12] A huge magnetoresistance has been observed in the case of n- and p-type Ag_2Te.[13,14] Bulk Ag_2Te is known to show a thermoelectric effect. Its Seebeck coefficient was studied in the temperature range of 2−450 K.[15] The values of n- and p-type Ag_2Te were investigated in the range of 55−300 K.[16] Aliev et al. studied this in the temperature range of 80−300 K and explained the data on the basis of carrier-scattering mechanism.[17] Seebeck coefficients of vacuum-evaporated thin films were −110 and 130 μV K^{-1} in the thicknesses of 58 and 41 nm, respectively.[18,15] Recently, Li et al. found a maximum Seebeck coefficient of −170 μV K^{-1} for 1D Ag_2Te NWs.[9] Magnetic field dependent magnetothermopower was found in p-type $Ag_{2-\delta}Te$, which shows a maximum value at 7 T.[19] The ability of nanomaterials to exhibit an enhanced thermoelectric effect is thought to be very significant toward the development of high-efficiency devices and sensors.

Bulk Ag_2Te is prepared by the solid-state reaction between elemental silver and tellurium at high temperature.[20] Ag_2Te nanostructures with different morphologies have been reported. Ag_2Te nanocrystals were synthesized by the ultrasonication of a $AgNO_3$ and Te mixture in ethylenediamine[21] and the sonication of Te and silver acetate in ethylene glycol.[22] The rodlike structure of Ag_2Te was synthesized by the reaction of AgCl and Te powder in mixed solvents, such as ethylenediamine and hydrazine hydrate.[23] Ag_2Te nanotubes have been synthesized hydrothermally, when sodium tellurate (Na_2TeO_3) and $AgNO_3$ in hydrazine/ammonia mixture were autoclaved at 393 K.[8] Ag_2Te NWs were obtained by cathodic electrolysis in dimethyl sulfoxide solutions containing $AgNO_3$ and $TeCl_4$ using porous anodic alumina membrane as the template.[11] Recently, Ag_2Te NWs were synthesized by a composite-hydroxide-mediated (CHM) method, where $AgNO_3$ and Te powder were heated at 498 K in a Teflon vessel containing ethylenediamine and hydrazine hydrate.[9] The synthesis of Ag_2Te nanorods in a reaction of Te nanorods and $AgNO_3$ in hydrazine and Na_2EDTA at 333 K has been reported.[24] In this report, we demonstrate a room-temperature solution-phase route for the synthesis of Ag_2Te NWs by the direct reaction of Te NWs with $AgNO_3$. Electrical resistance and Seebeck coefficient of Ag_2Te NWs were measured as the function of temperature. In addition, the surface-enhanced Raman scattering (SERS) property of Ag_2Te NWs was studied, and a sensitivity up to 10^{-7} M was observed using crystal violet (CV) as the analyte molecule. We believe that this is the first report of room-temperature solution-phase synthesis of Ag_2Te NWs, enabling further studies and applications.

Experimental Section

Sodium dodecyl sulfate (SDS, $C_{12}H_{25}O_4SNa$, 99%) was obtained from Acros. Tellurium dioxide (TeO_2, 99.9%) powder was purchased from Alfa Aesar. $AgNO_3$ and hydrazine monohydrate ($N_2H_4 \cdot H_2O$, 99−100%) were purchased from SD Fine

* To whom correspondence should be addressed. E-mail: pradeep@iitm.ac.in. Fax: 91-44-2257-0545/ 0509.

10.1021/jp901953f CCC: $40.75 © 2009 American Chemical Society
Published on Web 07/08/2009

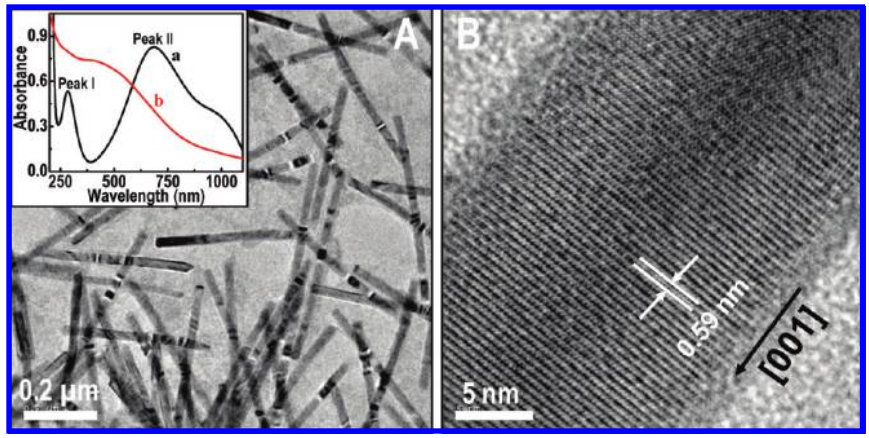

Figure 1. TEM images at different magnifications. (A) Large area image of Te NWs and (B) lattice-resolved image of a single Te NW. The inset of (A) shows UV−visible spectra of Te NWs (a) and Ag_2Te NWs (b).

Downloaded by INDIAN INST OF TECH MADRAS on July 31, 2009
Published on July 8, 2009 on http://pubs.acs.org | doi: 10.1021/jp901953f

Chemicals, India. CV was purchased from CDH, India. Deionized water was used throughout the experiment.

Ag_2Te NWs were synthesized by two steps: (1) synthesis of Te NWs and (2) reaction between Te NWs and $AgNO_3$. Te NWs were prepared by the chemical method reported by Chang et al.[25] In a reaction, 16 mg of TeO_2 powder was slowly added to a beaker containing 10 mL of hydrazine hydrate. The reaction was allowed to continue at room temperature under constant stirring. The powder was completely dissolved, and the color of the solution changed from colorless to blue after 1 h. The blue color indicates the formation of Te NWs. After 1 h, the solution was diluted 10-fold with 10 mM SDS, to control the length of the NWs. The as-prepared solution was purified by centrifugation at 18 000 rpm for 10 min to remove excess hydrazine and SDS. The residue was redispersed in deionized water and centrifuged twice for the complete removal of unreacted species.

To 90 mL of the purified Te NWs was added 10 mL of $AgNO_3$ (10 mM), and it was stirred for 12 h. The color changed from blue to black. The product was centrifuged at 18 000 rpm for 10 min, and the process was repeated twice for the complete removal of unreacted species. The residue was redispersed in deionized water for further characterization. Ag_2Te NW powder was prepared by freeze-drying the concentrated solution.

Instrumentation

UV−visible absorption spectra were recorded using a PerkinElmer Lambda 25 spectrophotometer. High-resolution transmission electron microscopy (HRTEM) and energy-dispersive X-ray analysis (EDAX) were carried out with an Oxford EDAX housed in a JEOL 3010, 300 kV instrument equipped with a UHR pole piece. The samples were prepared by dropping the dispersion on carbon-coated copper grids and drying in ambience. Scanning electron microscopy (SEM) and EDAX were carried out using an FEI QUANTA-200 SEM instrument, and the samples were prepared on conducting ITO glass plates. Differential scanning calorimetry (DSC) was carried out using a NETZSCH DSC 204 instrument under nitrogen atmosphere, at a heating rate of 10 K/min. X-ray diffraction (XRD) data were collected with a Shimadzu XD-D1 diffractometer using Cu Kα ($\lambda = 1.54$ Å) radiation. The samples were scanned in the 2θ range from 10 to 90 deg. All the peaks were assigned and compared with the database published by the Joint Committee on Power Diffraction Standards (JCPDS). X-ray photoelectron spectroscopy (XPS) measurements were done using an Omicron ESCA Probe spectrometer with monochromatized Al Kα X-rays ($h\nu = 1486.6$ eV). SERS spectra were studied by using a WiTec GmbH confocal micro Raman equipped with a CCD detector. The light source was a Nd:YAG laser of 532 nm wavelength. The electrical resistance was measured by the four-probe method. The Seebeck coefficient was measured on a pellet of 3 mm diameter and 8 mm length. The Seebeck coefficient was measured as a function of hot-end temperature, while the cold-end temperature was constant at 300 K.

Results and Discussion

The absorption spectra of Te NWs and Ag_2Te NWs were measured. The Te NWs have two characteristic peaks: peak I and peak II. Peak I is due to the transition from p-bonding valence band (VB2) to the p-antibonding conduction band (CB1), and it appears in the range of 250−350 nm. Peak II is due to the transition from p-lone pair valence band (VB3) to the p-antibonding conduction band (CB1), and it appears around 600−850 nm.[25−27] In a particular synthesis, peak I appeared at 284 nm and peak II appeared at 685 nm. The peak position changed for Ag_2Te NWs, which show a broad peak at 480 nm. The absorption spectra are shown in the inset of Figure 1A. The large area TEM image of the Te NWs is shown in Figure 1A. The length of the Te NWs was around 600 nm, and the width was around 20 nm. Figure 1B shows a lattice-resolved HRTEM image of a Te NW. The interplanar spacing is 0.59 nm, which corresponds to the (001) lattice plane of Te. All the NWs were straight and almost uniform in length. There were no dislocation and planar defects on the NWs, which suggests that it is single-crystalline.

After the addition of $AgNO_3$, the NWs changed to elongated bent structures retaining the aspect ratio of the parent NWs. Figure 2A shows the TEM image of bent Ag_2Te NWs, and Figure 2B shows the lattice-resolved HRTEM image of a single Ag_2Te NW. The interplanar spacing is 0.28 nm, which corresponds to the (220) lattice plane of Ag_2Te NW. The elemental analysis of Ag_2Te NW is shown in Figure 2C,D, which confirms the chemical composition. The atomic ratio of Ag to Te obtained from quantitative analysis of AgLα and TeLα in the EDS spectrum is 1.99:1, indicating a deficiency of silver in Ag_2Te.

The large area SEM image of Ag_2Te NWs is shown in Figure 3A. It reveals a similar morphology in accordance with TEM. Figure 3B shows the EDAX spectrum of Ag_2Te, indicating the presence of Ag and Te quantitatively. XRD patterns of the Te NWs and Ag_2Te NWs are shown in Figure 3C,D. All the peaks of Te NWs in the XRD pattern can be indexed to the hexagonal

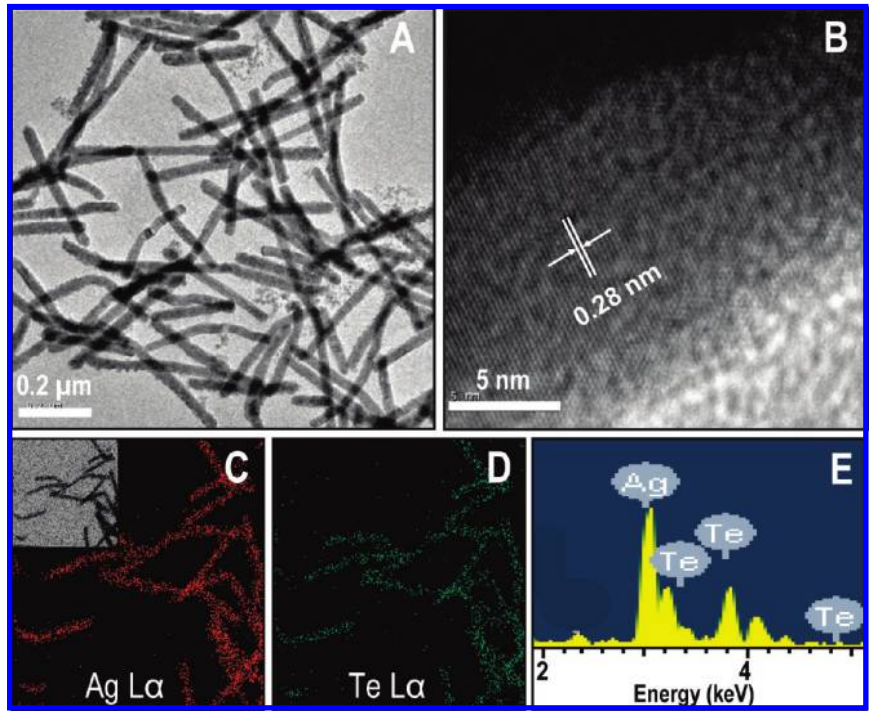

Figure 2. (A) Large area TEM image of Ag_2Te NWs, (B) lattice-resolved HRTEM of a single Ag_2Te NW, (C) elemental mapping using Ag and (D) Te, and (E) EDAX spectrum of Ag_2Te NWs. The TEM image corresponding to the elemental maps of (C) and (D) is shown in the inset of (C).

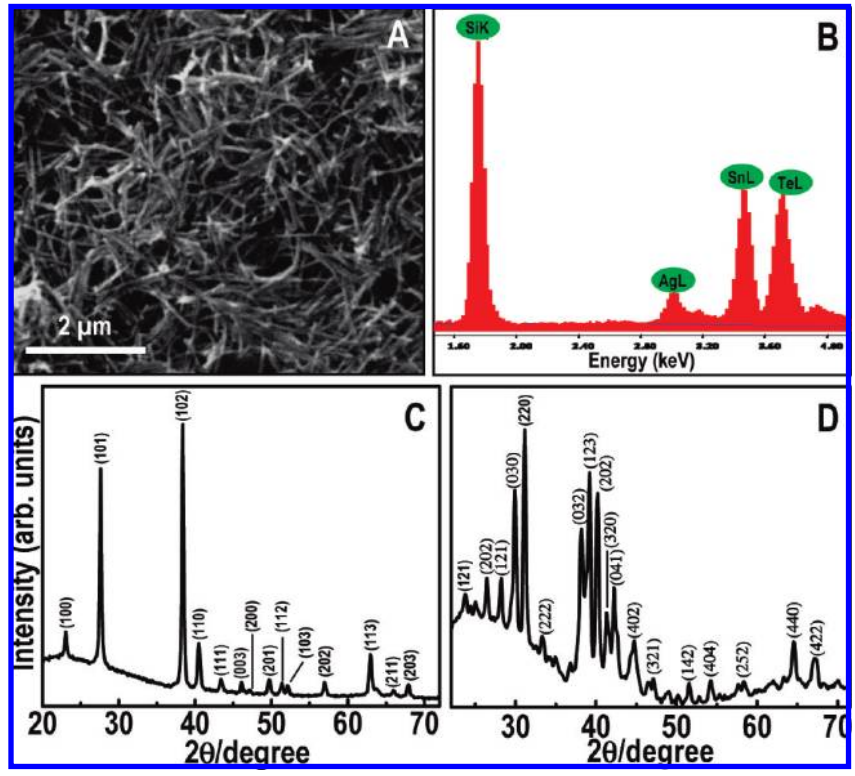

Figure 3. (A) SEM image of Ag_2Te NWs, (B) EDAX of Ag_2Te NWs showing the presence of Ag and Te, and (C) XRD pattern of Te NWs and (D) Ag_2Te NWs. Si and Sn in (B) are due to the substrate used.

phase of Te, whose unit cell constants are $a = 0.4451$ nm and $c = 0.5904$ nm, which is consistent with the literature data (JCPDS: 36-1452). All peaks in the XRD pattern are indexed to the monoclinic phase of Ag_2Te, whose unit cell constants calculated from diffraction peaks are $a = 0.8185$ nm, $b = 0.8934$ nm, $c = 0.8418$ nm and $\beta = 113.7°$, which is consistent with the literature data (JCPDS: 34-0142). The noticeable changes observed from the reactants to the products are that straight NWs got bent and a structural change occurred from a hexagonal phase to a monoclinic phase.

The structural phase transition from low temperature to high temperature was studied. The DSC of Ag_2Te NWs was measured under nitrogen atmosphere at a rate of 10 K/min. The data are shown in Figure 4A. The sample shows a structural phase transition from the low-temperature monoclinic structure (β-Ag_2Te) to the high-temperature face-centered cubic structure

Downloaded by INDIAN INST OF TECH MADRAS on July 31, 2009
Published on July 8, 2009 on http://pubs.acs.org | doi: 10.1021/jp901953f

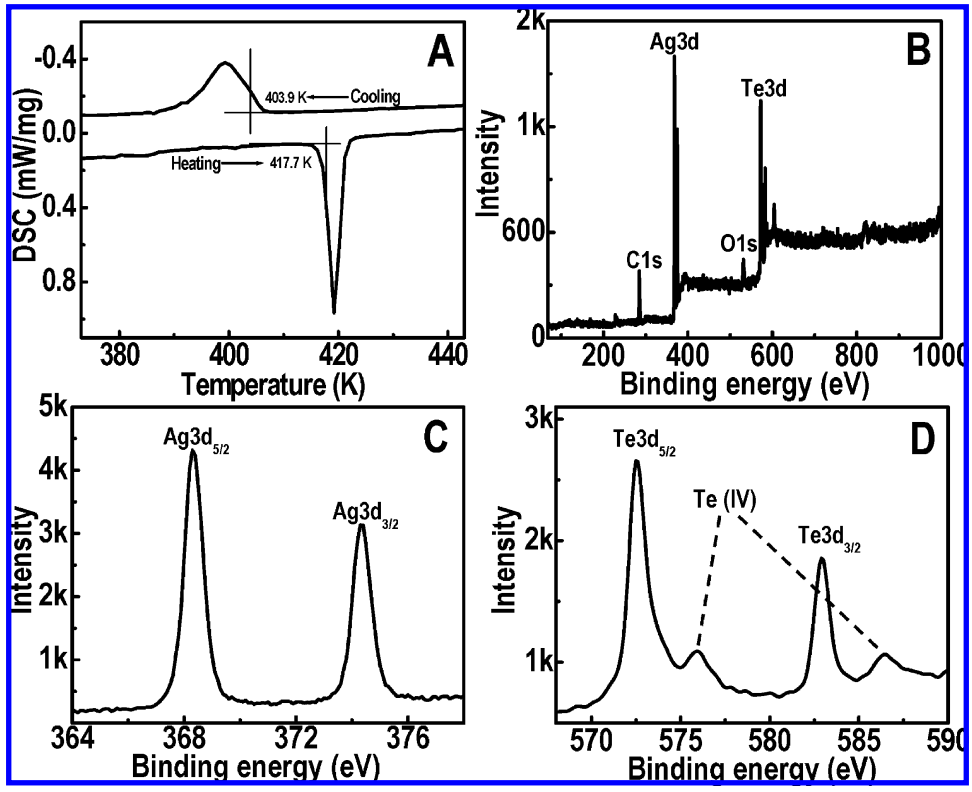

Figure 4. (A) DSC curves of Ag_2Te NWs, (B) XPS survey spectrum of Ag_2Te NWs, and (C) expanded scans in the Ag 3d and (D) Te 3d regions.

Downloaded by INDIAN INST OF TECH MADRAS on July 31, 2009
Published on July 8, 2009 on http://pubs.acs.org | doi: 10.1021/jp901953f

(α-Ag_2Te). During heating, a sharp peak was observed at 417.7 K, indicative of the endothermic structural phase transition from monoclinic to face-centered cubic phase. During cooling, an exothermic peak centered at 403.9 K was observed, attributed to the reverse transition. Structural phase transition during heating occurs over a narrow temperature window than the reverse transition. The latent heat of the phase transition, calculated from the DSC plot, was 14.53 J/g, lower than that observed for bulk (23.12 J/g) and thin film (25.75 J/g) samples.[28,15] Kinetics of the cubic-to-monoclinic transition is known to be slower than that of the reverse, explaining the broad DSC feature.

The chemical composition of the sample was confirmed from the XPS spectrum. XPS data reveal the presence of Ag and Te (Figure 4B). The peaks at 368.3 and 572.5 eV correspond to Ag $3d_{5/2}$ and Te $3d_{5/2}$, respectively, which indicate that Ag_2Te has Ag(+1) and Te(−2) valence states. The peaks at 368.3 and 374.3 eV correspond to Ag $3d_{5/2}$ and Ag $3d_{3/2}$, respectively (Figure 4C), and those at 572.5 and 582.9 eV correspond to Te $3d_{5/2}$ and Te $3d_{3/2}$, respectively (Figure 4D). Along with two main tellurium peaks, two small peaks are observed at 576.1 and 586.4 eV, which can be attributed to Te(IV) oxide. The XPS data are similar to those reported previously.[29,30] The quantification of peaks indicates a stoichiometry ratio of Ag to Te of 2:1.

Ag_2Te is a semiconductor in the monoclinic low-temperature phase and is metallic in the high-temperature cubic phase.[10] On heating, resistance decreases with increase in temperature in the monoclinic phase, and subsequently, upon increasing the temperature further, it increases with the nucleation of the cubic phase.[9,10] An abrupt increase in resistance was observed as the monoclinic phase changes to the cubic phase.[15] During cooling, a similar trend was observed, but the temperature of the phase change was different from that on heating. We measured temperature-dependent resistance during cooling (Figure 5, red

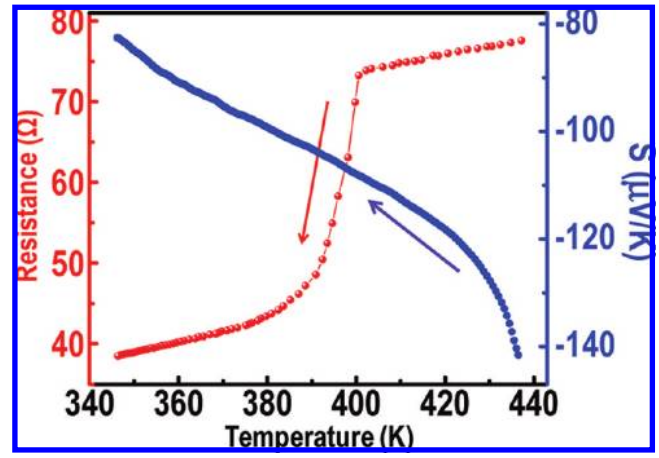

Figure 5. Resistance (red circles) and Seebeck coefficient (blue circles) of Ag_2Te NWs. Both the data were measured during cooling.

circles). It is found that the resistance decreases with temperature due to decrease in ionic conductivity in the cubic phase. At ~403 K, which is the phase transition temperature, the resistance decreases continuously over a wide temperature window. This temperature-dependent resistance data are similar to those reported earlier.[9,10,15] The Seebeck coefficient was also measured during cooling (Figure 5, blue circles). It was determined from the derivative of the thermal emf. The maximum Seebeck coefficient was found to be $-142\ \mu V\ K^{-1}$. A large value for the Seebeck coefficient was seen in the cubic phase, and it decreases with decrease in temperature, as the phase transition occurs. The negative Seebeck coefficient implies that electrons are the charge carriers.[28] It is known that the Seebeck coefficient is strongly dependent on the electronic conductivity.[9,31] The large Seebeck coefficient observed in the cubic phase is due to the increase in electronic and ionic conductivity.

The Raman spectra of Te NWs and Ag_2Te NWs were measured. The data are shown in Figure 6A. Te NWs show

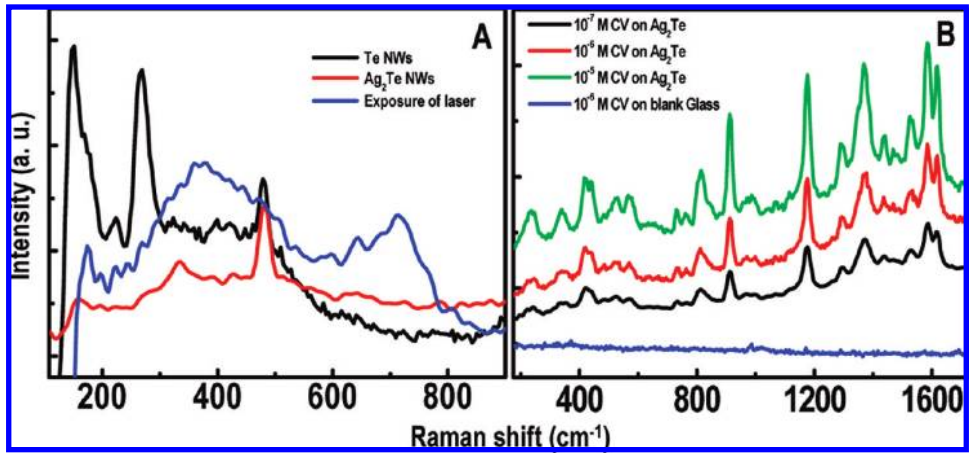

Figure 6. (A) Raman spectra of Te NWs and Ag_2Te NWs and (B) SERS spectra of CV at different concentrations on Ag_2Te NWs.

three intense peaks at 149, 267, and 479 cm^{-1}, whereas Ag_2Te NWs show a peak at 481 cm^{-1}. The peak at 149 cm^{-1} is due to the lattice vibration of Te NWs. The peak at 267 cm^{-1} can be assigned either to the Te−O vibration[32] of the thin oxide layer or to the Te−sulfate vibration arising from the stabilizing SDS. The peak at 479 cm^{-1} is due to the Te−O vibration of the oxide layer. On exposure of laser on Ag_2Te for 10 min, the peak at 481 cm^{-1} disappeared and two broad peaks at 392 and 712 cm^{-1} appeared. These two broad peaks are assigned to the bending and symmetric stretching modes of Te−O of TeO_2.[8] Upon laser exposure, Ag_2Te NWs may undergo surface oxidation, forming TeO_2 and silver. It is known that silver chalcogenides are sensitive to laser beams and cause a redox reaction, forming TeO_2.[33] Similar results have been obtained when Ag_2Te nanotubes were exposed to a laser for a long time.[8]

SERS is one of the most sensitive analytical tools to provide vibrational information when molecules are adsorbed onto metallic nanostructures.[34,35] A wide variety of silver systems, such as silver colloids, silver aggregated sols, periodic array of silver particles, and silver thin films, are known to show high SERS activity.[34,36] SERS is highly morphology-dependent with the electromagnetic enhancement being the dominant mechanism.[36] The polarization dependence of SERS of silver NWs, such as aligned NW rafts,[37] NW bundles,[38,39] coupled NWs,[40] and single NWs,[41] has been studied. Recently, gold−tellurium hybrid material was used as a SERS-active substrate.[42] We studied the SERS activity of the as-prepared Ag_2Te NWs using crystal violet (CV) as the analyte molecule at different concentrations. The enhancement is expected to be maximum at the junction between two adjacent nanoparticles. These sites are often called as "hot spots".[39,43,44] Confinement of the molecules in these hot spots is likely the reason for the SERS activity.

For the SERS measurements, the Ag_2Te NW substrate was immersed in CV solution of varying concentrations for 3 h. The substrate was washed gently with distilled water and dried. Figure 6B shows the Raman spectra of CV at different concentrations adsorbed on Ag_2Te NWs as well as on a blank glass substrate. The Ag_2Te NWs showed distinct Raman features of adsorbed CV even at a concentration of 10^{-7} M. At the same time, no Raman features were observed from the surface of the blank glass plate even at a higher concentration of CV (10^{-6} M). This indicates the good SERS activity of Ag_2Te NWs. The enhancement may be explained on the basis of an electric field generated near the Ag_2Te NWs when it interacts with the electromagnetic radiation. Uniformly distributed Ag on the NWs may provide efficient SERS-active sites. It is likely that two NWs can come together and can arrange in an end-to-end, sidewise, or crosswise manner, after drying on the cover glass. It has been proposed theoretically that the high SERS activity of silver nanowires is due to the electric field generated at the tips of the nanowires upon irradiation with light.[45] The junction created between the tip of the two nanowires, when it aligns in an end-to-end manner, can act as a SERS hot spot. SERS activity at these hot spots decreases as the interparticle distance increases. The large electromagnetic magnetic field generated at the tip can enhance the SERS intensity of the analyte molecules located at these junctions. Similarly, the sidewise enhancement of the NWs can be explained on the basis of pairwise electromagnetic interaction, when NWs are present in sufficiently small distances.[40] Enhancement can happen in a crosswise arrangement as well.[46]

Conclusion

Ag_2Te NWs were synthesized at room temperature using Te NWs as the template. The material was characterized by microscopic and spectroscopic tools. XRD analysis showed the formation of the monoclinic phase. HRTEM, SEM, EDAX, and XPS reveal that the composition of the material is close to Ag_2Te. The structural phase transition from low-temperature monoclinic phase to high-temperature face-centered cubic phase was seen at 417.7 K. The electrical resistance and Seebeck coefficient of the material were studied. The Seebeck coefficient was found to be ~142 $\mu V\ K^{-1}$. The SERS enhancement of Ag_2Te NWs was investigated using CV as the analyte, and a sensitivity up to 10^{-7} M was observed. SERS activity of a semiconducting nanomaterial opens up newer possibilities for sensors. Tuning the SERS activity of the material by tuning its conductivity (and, thereby, the electromagnetic field around it) may provide new avenues for research.

Acknowledgment. We thank the Nano Mission of the DST, Government of India, for supporting our research program. Kishnendu Biswas, IIT Madras, is thanked for the Seebeck coefficient measurement. P. Venkateshan and Prof. A. M. Umarji, Indian Institute of Science, Bangalore, are thanked for the resistance measurement.

References and Notes

(1) Cobden, D. H. *Nature* **2001**, *409*, 32.
(2) Cui, Y.; Lieber, C. M. *Science* **2001**, *291*, 851.
(3) Banerjee, S.; Dan, A.; Chakravorty, D. *J. Mater. Sci.* **2001**, *37*, 4261.
(4) Karakaya, I.; Thompson, W. T. *J. Phase Equilib.* **1991**, *12*, 56.
(5) Schneider, J.; Schulz, H. *Z. Kristallogr.* **1993**, *203*, 1.

Downloaded by INDIAN INST OF TECH MADRAS on July 31, 2009
Published on July 8, 2009 on http://pubs.acs.org | doi: 10.1021/jp901953f

(6) Manolikas, C. *J. Solid State Chem.* **1987**, *66*, 1.
(7) Das, V. D.; Karunakaran, D. *J. Appl. Phys.* **1989**, *66*, 1822.
(8) Qin, A. M.; Fang, Y. P.; Tao, P. F.; Zhang, J. Y.; Su, C. Y. *Inorg. Chem.* **2007**, *46*, 7403.
(9) Li, F.; Hu, C.; Xiong, Y.; Wan, B.; Yan, W.; Zhang, M. *J. Phys. Chem. C* **2008**, *112*, 16130.
(10) Gnanadurai, P.; Soundararajan, N.; Sooriamoorthi, C. E. *Phys. Status Solidi B* **2003**, *237*, 472.
(11) Chen, R.; Xu, D.; Guo, G.; Gui, L. *J. Mater. Chem.* **2002**, *12*, 2435.
(12) Kobayashi, M.; Ishikawa, K.; Tachibana, F.; Okazaki, H. *Phys. Rev. B* **1988**, *38*, 3050.
(13) Xu, R.; Husmann, A.; Rosenbaum, T. F.; Saboungi, M. L.; Enderby, J. E.; Littlewood, P. B. *Nature* **1997**, *390*, 57.
(14) Chuprakov, I. S.; Dahmen, K. H. *Appl. Phys. Lett.* **1998**, *72*, 2165.
(15) Gnanadurai, P.; Soundararajan, N.; Sooriamoorthy, C. E. *Vacuum* **2002**, *67*, 275.
(16) Wood, C.; Harrap, V.; Kane, W. M. *Phys. Rev.* **1961**, *121*, 978.
(17) Aliev, S. A.; Suyunov, U. K.; Aliev, M. I. *Sov. Phys. Semicond.* **1974**, *7*, 1383.
(18) Damodara, D. V.; Karunakaran, D. *Phys. Rev. B* **1984**, *30*, 2036.
(19) Sun, Y.; Salamon, M. B. *Appl. Phys. Lett.* **2003**, *82*, 1440.
(20) Coustal, R. *J. Chem. Phys.* **1958**, *38*, 277.
(21) Li, B.; Xie, Y.; Liu, Y.; Huang, J. X.; Qian, Y. T. *J. Solid State Chem.* **2001**, *158*, 260.
(22) Harpeness, R.; Palchik, O.; Gedanken, A.; Palchik, V.; Amiel, S.; Slifkin, M. A.; Weiss, A. M. *Chem. Mater.* **2002**, *14*, 2094.
(23) Jiang, Y.; Wu, Y.; Yang, Z. P.; Xie, Y.; Qian, Y. T. *J. Cryst. Growth* **2001**, *224*, 1.
(24) Zuo, P.; Zhang, S.; Jin, B.; Tian, Y.; Yang, J. *J. Phys. Chem. C* **2008**, *112*, 14825.
(25) Lin, Z. H; Yang, Z.; Chang, H. T. *Cryst. Growth Des.* **2008**, *8*, 351.
(26) Sreeprasad, T. S.; Samal, A. K.; Pradeep, T. *J. Phys. Chem. C* **2009**, *113*, 1727.
(27) Gautama, U. K.; Rao, C. N. R. *J. Mater. Chem.* **2004**, *14*, 2530.
(28) Aliev, S. A.; Aliev, F. F.; Gasanov, Z. S. *Phys. Solid State* **1998**, *40*, 1540.
(29) Bahl, M. K.; Watson, R. L.; Irgolic, K. J. *J. Chem. Phys.* **1977**, *66*, 5526.
(30) Song, J. M.; Lin, Y. Z.; Zhan, Y. J.; Tian, Y. C.; Liu, G.; Yu, S. H. *Cryst. Growth Des.* **2008**, *8*, 1902.
(31) Park, K.; Jang, K. U.; Kwon, H. C.; Kim, J. G.; Cho, W. S. *J. Alloys Compd.* **2006**, *419*, 213.
(32) Baesman, S. M.; Bullen, T. D.; Dewald, J.; Zhang, D.; Curran, S.; Islam, F. S.; Beveridge, T. J.; Oremland, R. S. *Appl. Environ. Microbiol.* **2007**, *73*, 2135.
(33) Henshaw, G.; Parkin, I. P.; Shaw, G. A. *J. Chem. Soc., Dalton Trans.* **1997**, 231.
(34) Moskovits, M. *Rev. Mod. Phys.* **1985**, *57*, 783.
(35) Chang, R. K.; Furtak, T. E. *SurfaceEnhanced RamanScattering*; Plenum Press: New York, 1982.
(36) Campion, A.; Kambhampati, P. *Chem. Soc. Rev.* **1998**, *27*, 241.
(37) Jeong, D. H.; Zhang, Y. X.; Moskovits, M. *J. Phys. Chem. B* **2004**, *108*, 12724.
(38) Tao, A.; Kim, F.; Hess, C.; Goldberger, J.; He, R.; Sun, Y.; Xia, Y.; Yang, P. *Nano Lett.* **2003**, *3*, 1229.
(39) Lee, S. J.; Morrill, A. R.; Moskovits, M. *J. Am. Chem. Soc.* **2006**, *128*, 2200.
(40) Tao, A. R.; Yang, P. D. *J. Phys. Chem. B* **2005**, *109*, 15687.
(41) Mohanty, P.; Yoon, I.; Kang, T.; Seo, K.; Varadwaj, K. S. K.; Choi, W.; Park, Q. H.; Ahn, J. P.; Suh, Y. D.; Ihee, H.; Kim, B. *J. Am. Chem. Soc.* **2007**, *129*, 9576.
(42) Lin, Z. H.; Chang, H. T. *Langmuir* **2008**, *24*, 365.
(43) Gunnarsson, L.; Rindzevicius, T.; Prikulis, J.; Kasemo, B.; Kall, M.; Zou, S. L.; Schatz, G. C. *J. Phys. Chem. B* **2005**, *109*, 1079.
(44) Schuck, P. J.; Fromm, D. P.; Sundaramurthy, A.; Kino, G. S.; Moerner, W. E. *Phys. Rev. Lett.* **2005**, *94*, 017402.
(45) Hao, E.; Schatz, G. C. *J. Chem. Phys.* **2004**, *120*, 357.
(46) Kang, T.; Yoon, I.; Jeon, K. S.; Choi, W.; Lee, Y.; Seo, K.; Yao, Y.; Park, Q. H.; Ihee, H.; Suh, Y. D.; Kim, B. *J. Phys. Chem. C* **2009**, *113*, 7492.

JP901953F

Downloaded by INDIAN INST OF TECH MADRAS on July 31, 2009
Published on July 8, 2009 on http://pubs.acs.org | doi: 10.1021/jp901953f